The Impact of Antarctic Cloud Radiative Properties on a GCM Climate Simulation*

DAN LUBIN,[+] BIAO CHEN,[#] DAVID H. BROMWICH,[#,@] RICHARD C. J. SOMERVILLE,[&] WAN-HO LEE,[&,**] AND KEITH M. HINES[#]

[+]*California Space Institute, Scripps Institution of Oceanography, University of California, San Diego, La Jolla, California*
[#]*Polar Meteorology Group, Byrd Polar Research Center, Ohio State University, Columbus, Ohio*
[@]*Atmospheric Sciences Program, Ohio State University, Columbus, Ohio*
[&]*Climate Research Division, Scripps Institution of Oceanography, University of California, San Diego, La Jolla, California*

(Manuscript received 6 January 1997, in final form 27 May 1997)

ABSTRACT

A sensitivity study to evaluate the impact upon regional and hemispheric climate caused by changing the optical properties of clouds over the Antarctic continent is conducted with the NCAR Community Model version 2 (CCM2). Sensitivity runs are performed in which radiation interacts with ice clouds with particle sizes of 10 and 40 μm rather than with the standard 10-μm water clouds. The experiments are carried out for perpetual January conditions with the diurnal cycle considered. The effects of these cloud changes on the Antarctic radiation budget are examined by considering cloud forcing at the top of the atmosphere and net radiation at the surface. Changes of the cloud radiative properties to those of 10-μm ice clouds over Antarctica have significant impacts on regional climate: temperature increases throughout the Antarctic troposphere by 1°–2°C and total cloud fraction over Antarctica is smaller than that of the control at low levels but is larger than that of the control in the mid- to upper troposphere. As a result of Antarctic warming and changes in the north–south temperature gradient, the drainage flows at the surface as well as the meridional mass circulation are weakened. Similarly, the circumpolar trough weakens significantly by 4–8 hPa and moves northward by about 4°–5° latitude. This regional mass field adjustment halves the strength of the simulated surface westerly winds. As a result of indirect thermodynamic and dynamic effects, significant changes are observed in the zonal mean circulation and eddies in the middle latitudes. In fact, the simulated impacts of the Antarctic cloud radiative alteration are not confined to the Southern Hemisphere. The meridional mean mass flux, zonal wind, and latent heat release exhibit statistically significant changes in the Tropics and even extratropics of the Northern Hemisphere. The simulation with radiative properties of 40-μm ice clouds produces colder surface temperatures over Antarctica by up to 3°C compared to the control. Otherwise, the results of the 40-μm ice cloud simulation are similar to those of the 10-μm ice cloud simulation.

1. Introduction

Global climate modeling (GCM) studies over the past two decades have consistently shown that by improving the realism of cloud parameterizations, overall GCM performance is noticeably improved (e.g., Ramanathan et al. 1983; Slingo and Slingo 1991; Kiehl 1994; Lee and Somerville 1996). For example, one of the fundamental microphysical aspects of global cloud optical properties is a smaller effective droplet size over land versus over ocean (Han et al. 1994). In a study by Kiehl (1994), the standard cloud droplet effective radius of 10 μm in the National Center for Atmospheric Research (NCAR) Community Climate Model version 2 (CCM2) was replaced over land by a parameterization that allowed for smaller droplets as a function of temperature. This led to improvements of up to 20 W m^{-2} in the Northern Hemisphere shortwave cloud forcing as compared with Earth Radiation Budget Experiment (ERBE) data, a reduction in surface-absorbed solar fluxes over land of up to 5 W m^{-2}, a corresponding decrease in surface temperature over land by as much as 2.0–3.5 K, and a decrease in moisture flux into the atmosphere that in turn led to reductions in simulated precipitation of up to 12 mm day^{-1}. These results, most of which could be considered as improvements to CCM2 performance, were ultimately related to the larger shortwave reflectivity of the smaller liquid water droplets.

Recently some fundamental questions have been raised about the extent to which clouds absorb solar radiation (Cess et al. 1995; Ramanathan et al. 1995).

* Byrd Polar Research Center Contribution Number 1005.

** Current affiliation: Systems Engineering Research Institute, Taejon, Korea.

Corresponding author address: Dr. David H. Bromwich, Byrd Polar Research Center, Ohio State University, 1090 Carmack Road, 108 Scott Hall, Columbus, OH 43210-1002.
E-mail: bromwich@polarmet1.mps.ohio-state.edu

Standard (plane parallel) radiative transfer theory appears to underestimate global mean solar absorption by 25 W m^{-2} as compared with ERBE data and ground-based insolation measurements. Kiehl et al. (1995) inserted a parameterization for this observed ''excess cloud absorption'' into the NCAR CCM2. The resulting heating and moistening of the troposphere increased atmospheric stability, reduced convective heating, and ultimately reduced the strength of the Hadley circulation, which brought about reduced surface wind speeds and surface latent heat fluxes in the Tropics. Again, most of these results could be viewed as improvements to CCM2 in that they reduced known biases. It therefore appears that one must have some basic knowledge of cloud optical properties (opacity, effective particle size, emissivity, and solar absorptivity) in any given region if one expects the most accurate GCM simulation of the region's climate.

The one region where the ''excess cloud absorption'' reported by Cess et al. (1995) did not appear was over the Antarctic continent (i.e., in radiation measurements from the South Pole). The troposphere over the high Antarctic plateau exhibits a combination of physical phenomena not found anywhere else. These include surface air temperatures routinely below -50°C (e.g., Keller et al. 1989), water vapor abundance rarely above 600 precipitable μm (Zav'yalova 1986), and a radiative cooling effect of CO_2 rather than a warming effect as illustrated by the satellite-based infrared emission spectra in Hanel et al. (1972). In the presence of strong temperature inversions in the lower troposphere over much of the Antarctic continent, clouds warm the surface and cool the free atmosphere (Yamanouchi and Charlock 1995); this climatic effect of cloud cover is rarely found anywhere else. In addition, the very small tropospheric water vapor burden over Antarctica implies a more important radiative and thermodynamic role of clouds relative to trace gas emission and absorption (Walden 1995).

Compared to most other regions of the world, our knowledge about the optical and microphysical properties of Antarctic cloud cover is sparse. Over the Southern Ocean, Fourier Transform Infrared (FTIR) atmospheric longwave emission spectra suggest that the persistent stratiform water clouds have effective particle radius mostly in the range 9–11 μm, as one might expect for maritime cloud cover (Lubin 1994). In situ microprobe measurements of clouds between 75° and 80°S over the Ross Ice Shelf and Ross Sea by Saxena and Ruggiero (1990) revealed tenuous water clouds (liquid water content around 0.1 g m^{-3}) having a bimodal droplet size distribution with effective radius in the range 6.5–8.5 μm. An aircraft lidar experiment deployed on summer supply flights between McMurdo Station (78°S, 165°E) and the South Pole showed an abrupt end to liquid water clouds at the Antarctic coastline and the persistence of ice crystal clouds in the lower troposphere over the Antarctic plateau (Morely et al. 1989). Analysis of South Pole radiometersonde data collected between 1959 and 1963 suggests that tropospheric ice clouds during winter have small ice water content ($3–60 \times 10^{-4}$ g m^{-3}), small effective particle radius for ice clouds (4–16 μm), moderate emissivity (of order 0.6), and shortwave optical depth of order 1 (Stone 1993). Analysis of Advanced Very High Resolution Radiometer infrared data covering the South Pole by Lubin and Harper (1996) suggests that, if clouds are composed of ice crystals, they have small effective particle radius (12 μm) during summer as well. These assorted investigations therefore suggest a transition from typical maritime stratiform (liquid water) clouds over the Southern Ocean, with an effective radius of 10 μm, to more tenuous liquid water clouds in Antarctic coastal areas south of 70°S and over the ice shelves, to clouds composed of relatively small ice crystals over the Antarctic continent. While much more field work is necessary to bring our understanding of Antarctic clouds to the level of, say, the tropical western Pacific Ocean, the above mentioned investigations provide a basis for some initial GCM sensitivity studies.

To date the few observations that exist of Antarctic cloud radiative properties have not been incorporated directly into GCM simulations of Antarctic climate. As one might expect, simulations of present-day Antarctic climate by CCM2 exhibit some biases related to cloud cover. Tzeng et al. (1994) diagnosed the NCAR CCM2 simulation of the modern Antarctic climate and found that CCM2 can well simulate many important regional features, including the circumpolar trough, the strength and areal extent of the surface inversion, and the arid climate over the continent. However, anomalously high cloud amounts are generated over the Antarctic continent on a year-round basis. This reduces the incoming solar radiation in summer, and thus the amount of energy absorbed by the snow surface. During November–February, the simulated surface air temperatures in the interior are up to 10°C too cold.

One study with an earlier and less sophisticated model than CCM2 did illustrate the radiative and dynamical implications of cloud parameterization on Antarctic climate simulation. Shibata and Chiba (1990) performed a 1-month integration for May with the Japanese Meteorological Research Institute global spectral model. Their longwave radiation scheme included a parameterization that assigned gray emissivities (less than unity, but constant in wavelength) to clouds as a function of cloud base temperature. The radiation scheme was found to play a critical role in the simulated surface temperature. In addition, the Antarctic surface temperature was found to be highly correlated with surface pressure, such that a few degrees warming over Antarctica accompanied large pressure rises poleward of 60°S with smaller falls farther north. Consequently, the circumpolar lows weakened and moved northward.

The study reported here illustrates the impact of a first-order refinement in the representation of Antarctic

clouds in CCM2: a change from the optical properties of 10-μm water clouds to those of small ice particle clouds over the Antarctic continent. These refinements demonstrate that changing Antarctic cloud radiative properties has significant impacts on climate simulation over the Antarctic continent (roughly the area south of 70°S in the zonal mean) and surrounding Southern Ocean. In addition, we find that the simulated impact of the Antarctic cloud radiative specification is not confined to the Southern Hemisphere and extends to the Tropics and extratropics of the Northern Hemisphere.

2. Approach

The standard CCM2 (Hack et al. 1993) prescribes the optical properties of water clouds with 10-μm effective radius everywhere. While the new CCM3 (Kiehl et al. 1996) allows for both ice and water clouds, here we are interested in the impact of making the cloud cover over Antarctica more realistic. For this experiment, we changed the optical properties of clouds over the Antarctic continent from water clouds to ice clouds, using both the shortwave and longwave parameterizations developed by Ebert and Curry (1992). This change is made only over the continent and not over the ice shelves or surrounding Southern Ocean. The cloud prediction schemes in CCM2 were left intact. No other changes were made to the climate model. In addition to a control simulation with water clouds, two experimental runs were performed: one with Antarctic clouds having radiative properties of ice particle effective radius of 10 μm and another with radiative properties of ice particle radius of 40 μm. The former was intended to represent the order of magnitude in particle sizes suggested by the experimental reports cited above. Because there is not yet enough field work to specify Antarctic cloud microphysics with as much certainty as at lower latitudes (although from the annual cycle in lower tropospheric temperatures over the continent we expect mainly ice clouds), we included the latter simulation to represent approximately the lower limit on ice cloud effective radius observed in lower latitude cirrus clouds (Knollenberg et al. 1993; Lubin et al. 1996). The shortwave parameterizations of single scattering albedo, asymmetry factor, and volume extinction as functions of particle effective radius developed by Ebert and Curry (1992) were incorporated directly into the CCM2 radiation code. The standard CCM2 assumes a gray longwave cloud emissivity based on clouds having a mass absorption coefficient of 0.1 $m^2\ g^{-1}$. Following Ebert and Curry (1992), we recomputed the mass absorption coefficient pertaining to the integrated longwave spectrum; the values are 0.188 $m^2\ g^{-1}$ for ice cloud effective radius of 10 μm and 0.050 $m^2\ g^{-1}$ for ice cloud effective radius of 40 μm.

The ice cloud parameterizations of Ebert and Curry (1992) purposely used the same mathematical formalism as those developed by Slingo (1989) for liquid water clouds. The latter was incorporated directly into CCM2 for shortwave radiative flux computation. For a fixed effective radius of 10 μm, the change in refractive index from liquid water to ice increases the optical depth by more than 50% throughout the shortwave (for fixed cloud water path). This change in refractive index also decreases the single scattering albedo in the near infrared, and decreases the scattering asymmetry factor between wavelengths 0.7–1.9 μm (the part of the near infrared containing the most solar energy). When the liquid water cloud with effective radius of 10 μm is changed to an ice cloud having effective radius of 40 μm, the optical depth decreases by more than 2.5 throughout the shortwave (for a fixed cloud water path). For the 40-μm ice cloud, the single scattering albedo between wavelengths 0.7–1.9 μm is slightly smaller than that of the 10-μm ice cloud, while the scattering asymmetry factor is slightly larger. At fixed cloud optical depth, either a smaller single scattering albedo or a smaller asymmetry factor will generally mean that less solar flux reaches the surface. However, these are second-order effects in the global climate simulation. What matters most in CCM2 is the cloud optical depth at fixed cloud water path, and the large changes in this quantity that we induced by switching from liquid water to ice were the primary influences on the shortwave flux in this set of experiments. The direct radiative effect in the control and experimental runs resulted from the value of the spectral optical depth (for a given cloud water path), single scattering albedo, asymmetry factor, and longwave mass absorption coefficient. In general, there will also be an indirect effect, as the radiative flux changes induce thermodynamic changes that feed back to alter the cloud fraction and cloud water path.

These experimental runs were carried out for perpetual January conditions (midsummer) in which all boundary conditions were fixed at the values for 15 January but with the diurnal cycle being simulated. These simulations were run for 12 perpetual months with the first 2 months being discarded due to adjustment to the initial conditions. These were compared to a control perpetual run which had the standard water cloud optical properties over all of Antarctica. The runs were done with a horizontal resolution of T42 (2.8° latitude $\times$ 2.8° longitude). It has been shown that this higher spatial resolution (as opposed to R15) is necessary to properly represent the complex terrain of Antarctica and avoid discrepancies related to geography (Bromwich et al. 1994; Tzeng et al. 1994; Chen et al. 1995).

3. Changes in cloud radiation and thermal forcing

The impact of these cloud changes on the Antarctic radiation budget can be demonstrated by examining both the cloud forcing at the top of the atmosphere (TOA) and the net radiation at the surface. The TOA shortwave cloud forcing is defined as the difference in net TOA

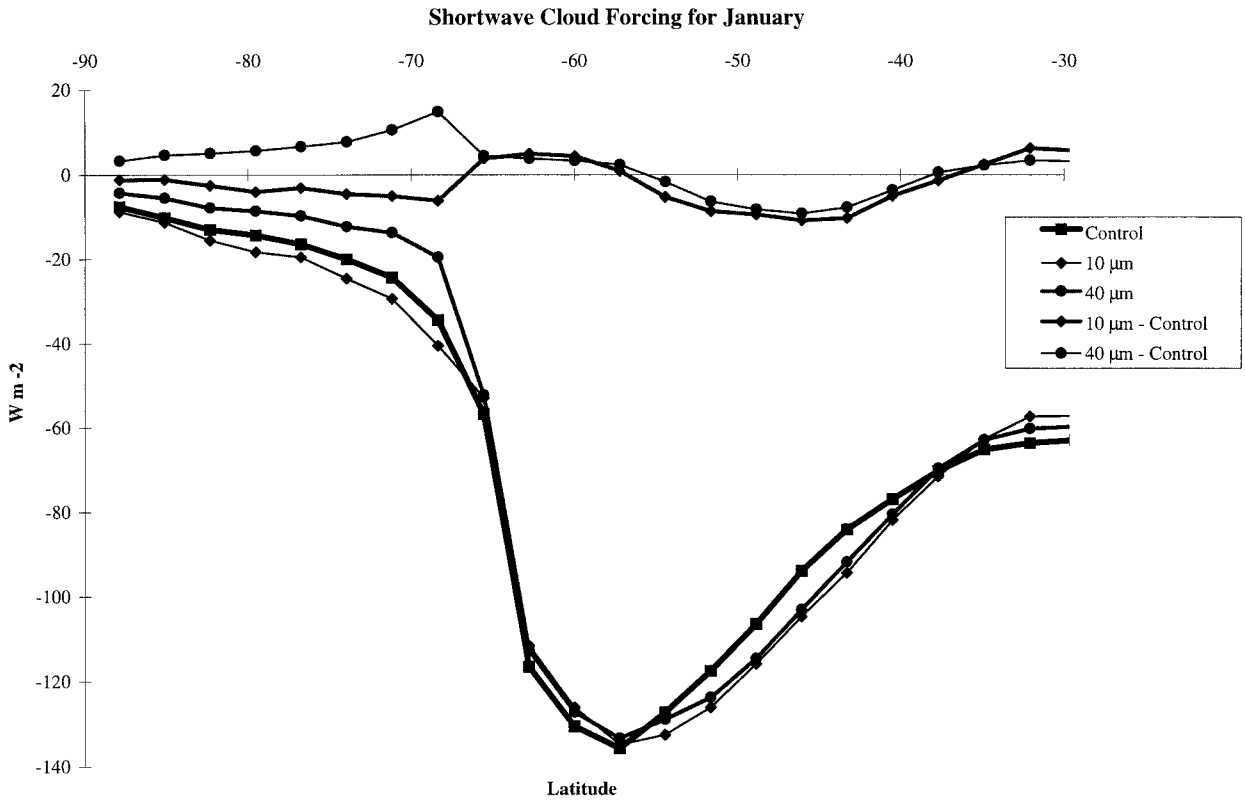

FIG. 1. Zonally averaged shortwave cloud forcing (W m^{-2}) at the top of the atmosphere in January for the control, 10- and 40-μm ice cloud runs, and differences between ice cloud runs and control run.

shortwave flux in the presence of cloud cover, S_{tot} and the net TOA shortwave flux over equivalent clear skies, S_{clr}:

$$\text{SWCF} = S_{tot} - S_{clr}. \quad (1)$$

The TOA longwave cloud forcing is defined as the difference between net TOA longwave flux over clear skies, F_{clr}, and the net TOA longwave flux in the presence of cloud cover, F_{tot}:

$$\text{LWCF} = F_{clr} - F_{tot}. \quad (2)$$

By collocating ERBE data with ground-based pyranometer and surface-albedo measurements at the South Pole, Nemesure et al. (1994) have demonstrated that cloud cover increases the planetary albedo over the Antarctic continent which means that the SWCF is negative and represents a cooling effect on the earth–atmosphere system. In all three CCM2 runs, the zonal mean SWCF is negative over the Antarctic continent (Fig. 1). Over the Antarctic continent, the SWCF for the 10-μm ice cloud run is within 3 W m^{-2} of the SWCF in the control run. The SWCF for the 40-μm ice cloud run is less negative than in the control run, because the increase in particle size and the change in optical properties decrease the shortwave cloud reflectance.

During the austral summer, the lowest layers of the troposphere over the Antarctic continent are either nearly isothermal or contain weak inversions, while most of the troposphere exhibits a temperature decrease with height. Hence, we expect the LWCF to be small. Figure 2 shows that the three GCM runs exhibit zonal mean LWCF values generally smaller than 15 W m^{-2} over the continent. The ice clouds with 10-μm effective radius exhibit a larger LWCF over the continent due to their larger emissivity for a given water content than either the 10-μm water clouds or the 40-μm ice clouds. Between 55°–70°S, the LWCF for either ice cloud case is up to 4 W m^{-2} smaller than in the control run due to the decreases in zonal mean cloud fraction in that region as shown later in Fig. 4. The total cloud fraction in the experimental runs is larger than in the control run farther north, and the zonal mean LWCF in either ice cloud run is up to 4 W m^{-2} larger than in the control run between 35°–55°S. Similar effects of cloud fraction over the Southern Ocean are also evident in the SWCF (Fig. 1), where the difference between the control run and either experimental run can be up to 10 W m^{-2}.

Figure 3 shows the zonally averaged net radiation balance at the surface along with the downward shortwave and upward longwave net surface radiation components. In the 10-μm ice cloud run, the net surface shortwave flux over the continent is 3–5 W m^{-2} smaller than in the control run. This relative reduction in zonally averaged surface insolation continues as far north as

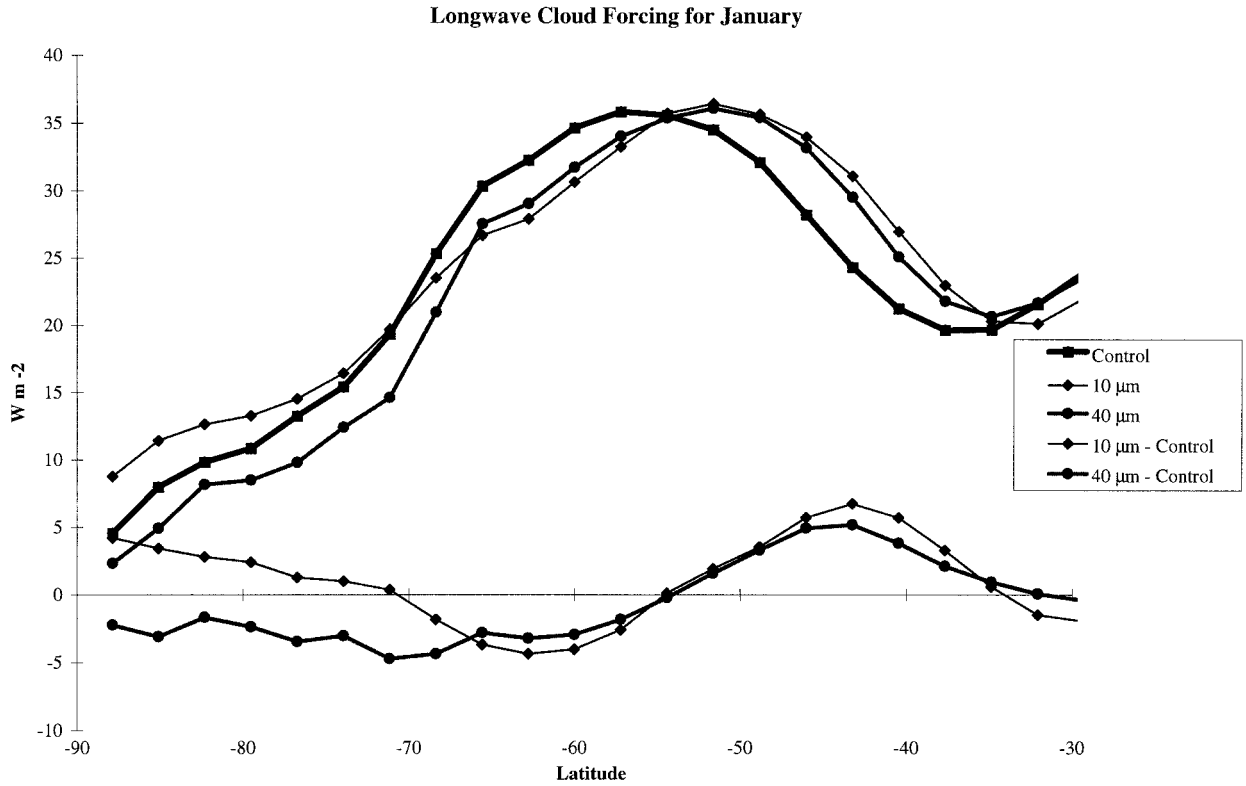

FIG. 2. Zonally averaged longwave cloud forcing (W m^{-2}) at the top of the atmosphere in January for the control, 10- and 40-μm ice cloud runs, and differences between ice cloud runs and control run.

66°S, even though the zonally averaged cloud fraction is reduced relative to the control north of 70°S. The smaller reflectivity of the 40-μm ice clouds over the continent brings about an increase in the zonally averaged net surface shortwave flux, relative to the control run, of 1–5 W m^{-2} at all southern high latitudes. The larger emissivity of the 10-μm ice clouds (for a given water content) causes the absolute value of the zonally averaged net longwave surface flux to be 2–5 W m^{-2} smaller than in the control run, from poleward of 70°S (i.e., more downward longwave flux is emitted to the surface). The smaller emissivity of the 40-μm ice clouds causes this same quantity to be around 2–3 W m^{-2} larger than in the control run over the continent, and due to differences in simulated cloud fraction, it remains this much larger at all southern high latitudes. The zonally averaged net surface radiation balance (sum of shortwave and longwave net surface fluxes) in the control run is zero at the South Pole and increases monotonically until 68°S. In the highest parts of the continental interior (85°–90°S), this same quantity in the 10-μm ice cloud run is positive (net energy gain by the surface), around 6–7 W m^{-2}, and then shows a monotonic increase northward that is essentially the same as in the control run until 82°S. Northward of this latitude, the zonally averaged net radiation balance is smaller in the 10-μm ice cloud run than in the control run. In the 40-μm ice cloud run, the zonally averaged net radiation balance is negative at the Pole (net energy loss by the surface), increasing northward to match the net radiation flux in the control run at 80°S and then remaining essentially the same as in the control run in the remaining continental latitudes. The gain of up to 7 W m^{-2} in the zonally averaged net radiation balance on the continent in the 10-μm ice cloud run, relative to the control run, is consistent with the surface temperature differences between these runs.

In both experimental runs, the zonally averaged total cloud fraction is slightly smaller than in the control run in the lowest tropospheric layers but is larger than in the control run in the middle to upper troposphere over interior Antarctica (Fig. 4). Statistical significance at the 95% confidence level via a *t*-test is demonstrated by shading for the difference fields in Figs. 4b and 4c. The total cloud fraction in both ice cloud runs is also slightly smaller than in the control run throughout the troposphere between 60°–70°S, generally where the continent meets the Southern Ocean. We do not necessarily expect large changes to the simulated cloud fraction, as we have changed only the cloud radiative properties and not any of the cloud prediction schemes in CCM2. Any change in the simulated cloud fraction must therefore come from indirect thermodynamic and dynamic effects. These small decreases in cloud fraction will detract from

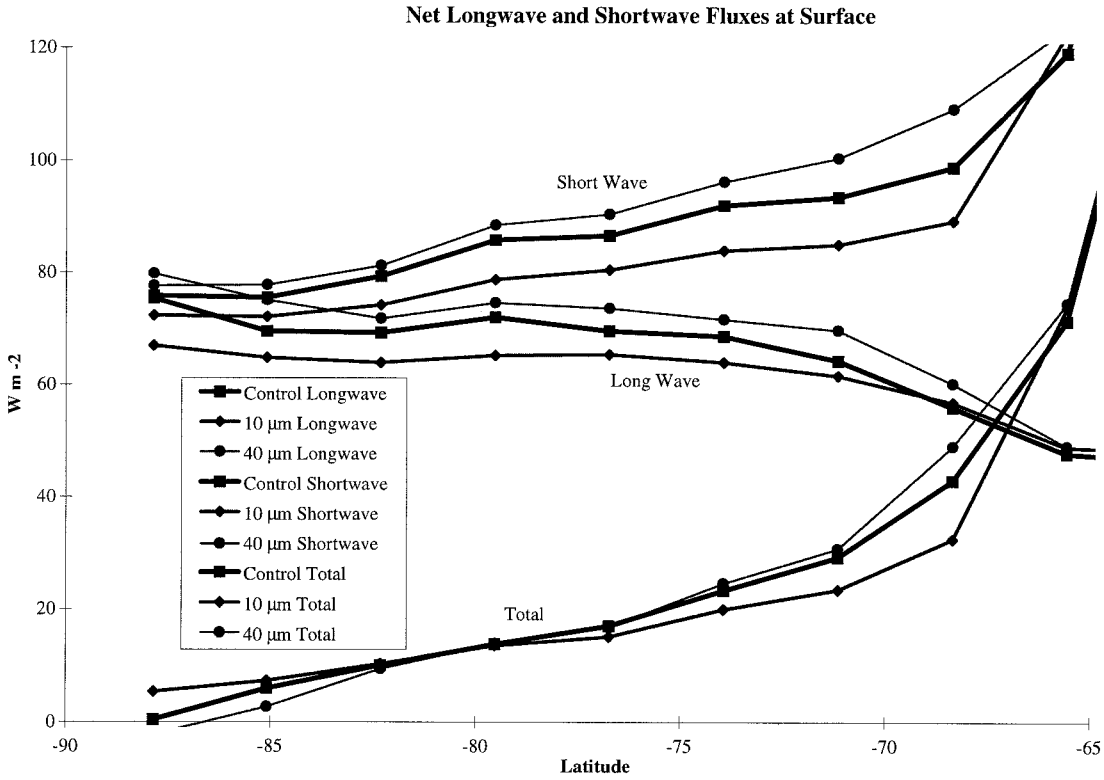

FIG. 3. Zonally averaged net upward longwave, downward shortwave, and downward total fluxes (W m^{-2}) at the surface in January for the control, 10- and 40-μm ice cloud runs.

the cloud radiative impact on the surface energy budget over the continent as discussed previously. These significant cloud fraction decreases, as well as the increases farther north (55°–40°S), will be discussed below in relation to the meridional circulation.

Figure 5 shows the model simulated surface temperature from the control run over all of Antarctica and the Southern Ocean along with similar contour plots of the difference in simulated surface temperature between the two experimental runs and the control run. The two experimental runs show opposite effects. Throughout most of the high Antarctic plateau, surface temperature is noticeably warmer in the 10-μm ice cloud run than in the control run. In many areas, this temperature difference is greater than 5 K. This suggests that, if Antarctic continental clouds are indeed more accurately characterized as ice clouds with 10-μm effective particle radius, this refinement alone removes approximately half of the surface temperature bias noted by Tzeng et al. (1994). The warning of the higher continental terrain in the 10-μm ice cloud run is accompanied by slight cooling (usually less than 0.5 K), relative to the control run, over the surrounding sea ice and ice shelves poleward of 70°S. The 40-μm ice clouds, in contrast, result in Antarctic plateau temperatures that are 2–3 K colder than in the control run. This cooling of the higher continental terrain is accompanied by surface warming (of up to 2 K) of the surrounding ocean and ice shelves poleward of 70°S.

Figure 6 shows the zonal mean differences in tropospheric temperature, between the experimental runs and the control run, as a function of altitude. In the zonal average, the 10-μm ice clouds result in a warmer Antarctic troposphere and surface by about 1 K. The use of 40-μm ice clouds results in a warmer Antarctic troposphere by about 1 K but a negligible change in the zonal mean surface temperature at Antarctic latitudes. The tropospheric warming in the 40-μm ice cloud run can be readily understood as resulting, at least in part, from radiation. Figure 1 shows that the 40-μm ice cloud reflects noticeably less radiation to space than either 10-μm cloud. This smaller absolute shortwave cloud forcing is a combination of two effects: (i) the larger particle size for a given cloud water content reduces the cloud albedo at conservative scattering wavelengths ($\lambda < 1$ μm), and (ii) near-infrared radiation ($\lambda > 0.7$ μm, which constitutes 40% of the sun's energy) is more strongly absorbed by larger particles in the ice phase. In addition, the 40-μm ice cloud has a smaller middle infrared emissivity for a given water content, and Fig. 2 shows that the impact of this emissivity difference is to reduce the longwave cloud forcing by 2–3 W m^{-2} over the continent. Thus, the 40-μm ice cloud run exhibits greater shortwave atmospheric heating and smaller longwave

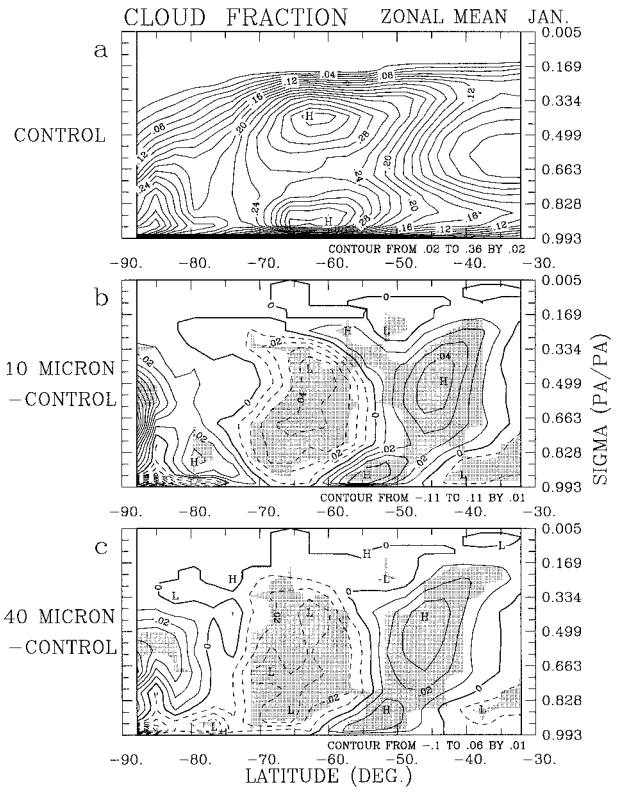

FIG. 4. Zonally averaged cross section of cloud fraction from 90°–30°S for January. (a) The control run, (b) difference between 10-μm ice cloud run and control run, and (c) difference between 40-μm ice cloud run and control run. Differences stippled in (b) and (c) are statistically significant at the 95% confidence level.

warming than either run with 10-μm cloud radius. A direct radiative contribution to the tropospheric warming in the 10-μm ice cloud run may be more subtle. Figure 1 shows that the shortwave cloud forcings for the 10-μm ice and water cloud runs are very similar, while the greater emissivity of the 10-μm ice cloud (for a given water content) results in a noticeably larger longwave cloud forcing (Fig. 2) by 3–5 W m^{-2} over the continent. While we certainly expect a heating of the surface to result from this larger longwave cloud forcing, we also expect the larger longwave cloud forcing to represent an atmospheric cooling in the case of a troposphere that is either near-isothermal or that has a temperature inversion. However, Fig. 6 shows that the CCM2 model troposphere over the continent exhibits a positive lapse rate during summer. In this case, a larger middle infrared cloud emissivity may contribute to a larger trapping of longwave radiation in the atmospheric layers beneath the cloud. In Fig. 4, we see that the 10-μm ice cloud run contains a larger cloud fraction than the control run in the mid- to upper troposphere (greatest statistical significance around 350 hPa) and a smaller cloud fraction near the surface. This tendency toward higher cloud layers (which also appears in the 40-μm ice cloud run) should represent an increase in the tropospheric longwave greenhouse effect. For the 10-μm ice cloud run, there is a warming anomaly centered at 70°S in the middle troposphere and a cooling anomaly center at 45°S in the upper troposphere, whereas at the surface there is warming at the South Pole and cooling for 50°–60°S. Thus, the zonally averaged meridional temperature gradient also changes (Fig. 7). The high latitude baroclinic zone has moved slightly poleward, and the midlatitude one has moved equatorward by about 5° due to the substantial reduction of the tropospheric meridional temperature gradient from 70°–45°S. We will discuss the related changes in the zonal wind in the next section.

4. Response in mean circulation and eddy flux

The changes to ice cloud radiative properties over the continent have a surprisingly large impact on sea level pressure over the Southern Ocean. Figures 8a and 8b show the sea level pressure in the control run and in ECMWF analyses, and Figs. 8c and 8d show the differences in surface pressure between the two experimental runs and the control run. The control run contains an adequate representation of both the location and strength of the circumpolar trough. Both experimental runs contain representations of the circumpolar trough that are less accurate. In both cases, the circumpolar trough is shifted northward and weakened. These effects are greater in the 10-μm ice cloud case, where the circumpolar lows are located 5° farther north than those in the control run, and are weaker by 5–9 hPa (i.e., contain higher surface pressures). Two regions around 65°S, where the location of the circumpolar lows have changed the most, show differences of 12 hPa in surface pressure between the 10-μm run and the control run. Shibata and Chiba (1990) noted that when they substituted nonblack clouds for blackbody clouds in their simpler GCM, the location of the circumpolar trough moved closer to the Antarctic continent; this was associated with colder continental temperatures under the nonblack clouds. Here in the 10-μm ice cloud run we have effectively increased the longwave cloud emissivity. The changes to ice cloud radiative properties over the continent have a surprisingly large impact for a given ice water path, and the circumpolar lows move northward; our result thus is consistent with that of Shibata and Chiba (1990).

Figure 9 shows the wind vectors at the sigma level nearest to the surface ($\sigma = 0.9925$) for the control and 10-μm ice cloud runs. As expected from the sea level pressure field, the surface wind speed over the Southern Ocean halves in the ice cloud run and the speed maximum moves northward; this is evident in Fig. 9c, where easterly anomalies (6–7 m s^{-1}) prevail for 70°–45°S. The drainage flow over Antarctica is weakened and poleward anomalies dominate over the continent; this is associated with the surface warming (Fig. 5b) for the 10-μm ice cloud run. Zonally averaged meridional cir-

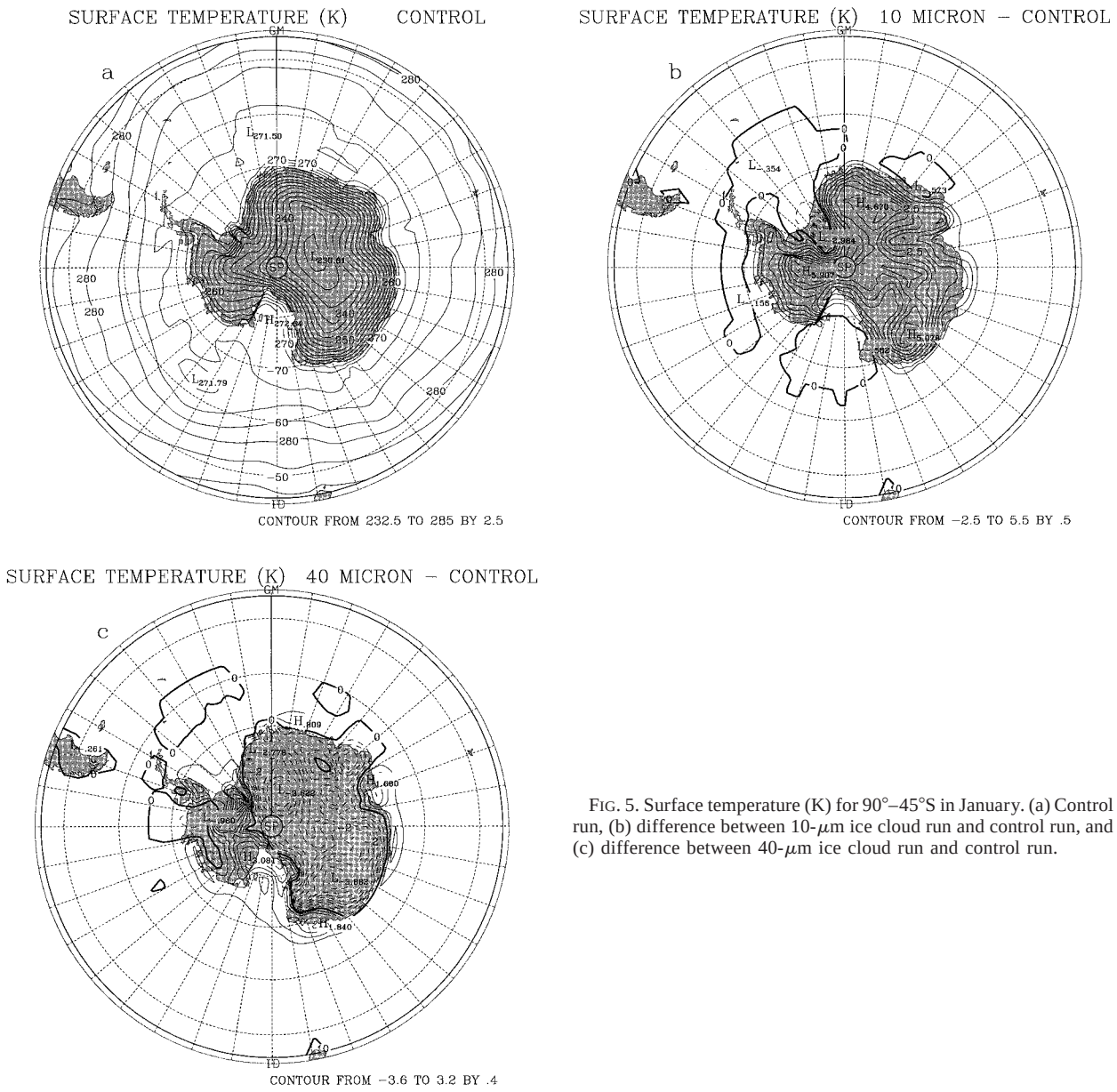

FIG. 5. Surface temperature (K) for 90°–45°S in January. (a) Control run, (b) difference between 10-μm ice cloud run and control run, and (c) difference between 40-μm ice cloud run and control run.

culation vectors (ω, v) are illustrated in Fig. 10 for the control and 10-μm ice cloud runs. There is a polar direct circulation that rises to the north of 65°S and sinks over the pole in the control (Fig. 10a). The indirect Ferrel circulation between 60°–30°S is centered near 48°S and the $\sigma = 0.6$ level. Both polar and Ferrel circulations in the 10-μm ice cloud run (not shown) are weakened in comparison to the control. From the difference in meridional circulations (Fig. 10b), it can be observed that there are reversed anomaly circulations in polar and middle latitude regions. These anomalies in sinking and rising motion from 90°–30°S are closely associated with cloud fraction anomalies (Fig. 4b), that is, less cloud coverage in 70°–55°S where the sinking anomalies occur and more cloud coverage in 50°–35°S where the rising motion anomalies appear. This suggests that the changes of cloud fraction in these regions are influenced by the mean meridional circulation anomalies that are adjustments to thermal structure changes induced by changes in cloud radiative properties over Antarctica. The vertical motion anomalies are also well correlated with temperature anomalies in Fig. 6b, with rising motion in the statically stable atmosphere resulting in cooling and sinking leading to warming.

The zonally averaged zonal wind component for the control and 10-μm ice cloud runs is shown in Fig. 11. During the southern summer, the subtropical and polar front jetstreams merge together and are centered near

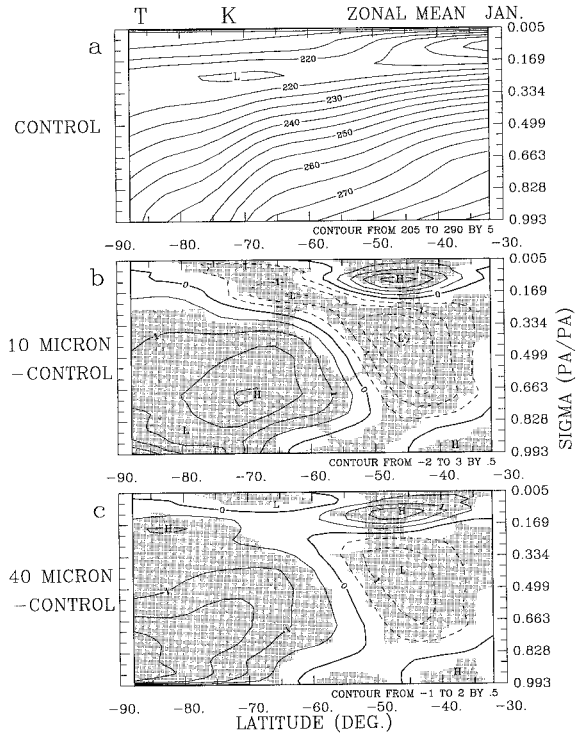

FIG. 6. Same as in Fig. 4 except for temperature (K).

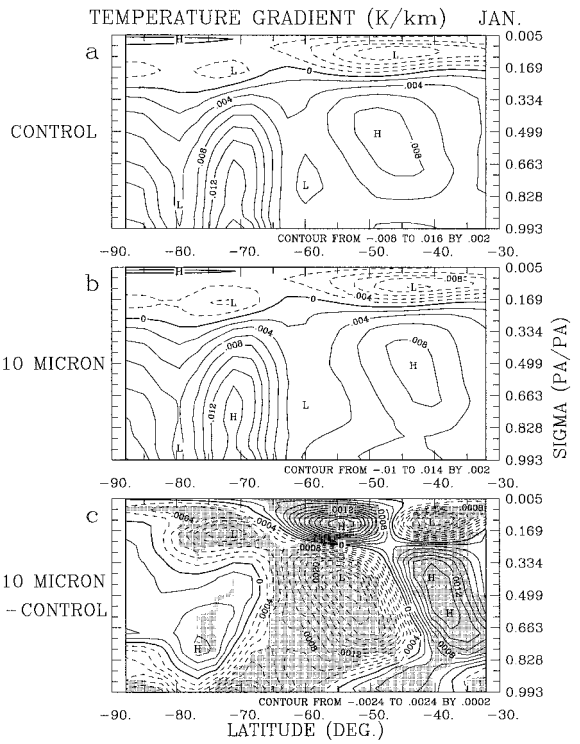

FIG. 7. Same as in Fig. 4 except for temperature gradient (K km^{-1}) for (a) control run, (b) 10-μm ice cloud run, and (c) differences between 10-μm ice cloud run and control run.

the $\sigma = 0.2$ level and 50°S in the control run. The subtropical and polar front jet streams separate from each other in the northern winter. In the 10-μm ice cloud run, the zonally averaged jet stream cores in both hemispheres are shifted equatorward by about 2.5° latitude; the north polar front jet becomes even more separated from the subtropical jet. It is worth pointing out that westerlies replace easterlies near the tropical tropopause. This change in the mean flow would allow wave anomalies in the Southern Hemisphere to propagate into the Northern Hemisphere (Webster 1983). We will examine this more in the next section. From the differences of zonal wind in Fig. 11c, easterly anomalies are observed in 70°–50°S where the maximum reduction of 10 m s^{-1} is located in the upper troposphere; westerly anomalies occur over Antarctica and 45°–25°S. There are also westerly increases in the northern Tropics and westerly decreases in the northern subtropics. All of the anomaly centers mentioned above are statistically significant.

We have seen that changes to ice cloud radiative properties over the Antarctic continent have substantial impacts on the mean circulations in the Southern Hemisphere summer as well as significant signals in the Northern Hemisphere winter. The fluxes of heat and momentum were further explored in terms of zonal means and deviations from zonal means in order to have a more integrated picture of changes that occurred in both eddy and mean fields due to modification of Antarctic cloud properties. Figure 12 shows the zonally averaged eddy heat fluxes. It is notable that in both hemispheres the midlatitude poleward eddy heat fluxes at lower levels are shifted poleward by about 15° latitude for the 10-μm ice cloud run in comparison to the control run. The eddy heat fluxes are much larger in the more zonally asymmetric northern winter than in the southern summer. As there is warming at the southern high latitudes and tropospheric cooling in the middle latitudes (section 3), this suggests that less poleward eddy heat flux is required to maintain the heat balance. In the Southern Hemisphere, there are two large equatorward eddy heat transport anomalies over Antarctica and 45°–25°S. The strongest poleward anomalies of eddy heat flux, however, appear 70°–45°S, where the largest reduction of the meridional temperature gradient occurs. There are also significant changes of eddy heat fluxes in the Northern Hemisphere: poleward anomalies of eddy heat flux in 50°–70°N and equatorward anomalies in 35°–50°N. In addition, and as expected, the anomalies of mean meridional heat flux (at least one order larger than eddy components, figure omitted) are in the same sense as the anomalies of meridional circulation; that is, the weakened Ferrel cell brings less warm air poleward at lower levels, while it transports less cold air equatorward in the upper troposphere.

The zonally deviated eddy momentum fluxes are dis-

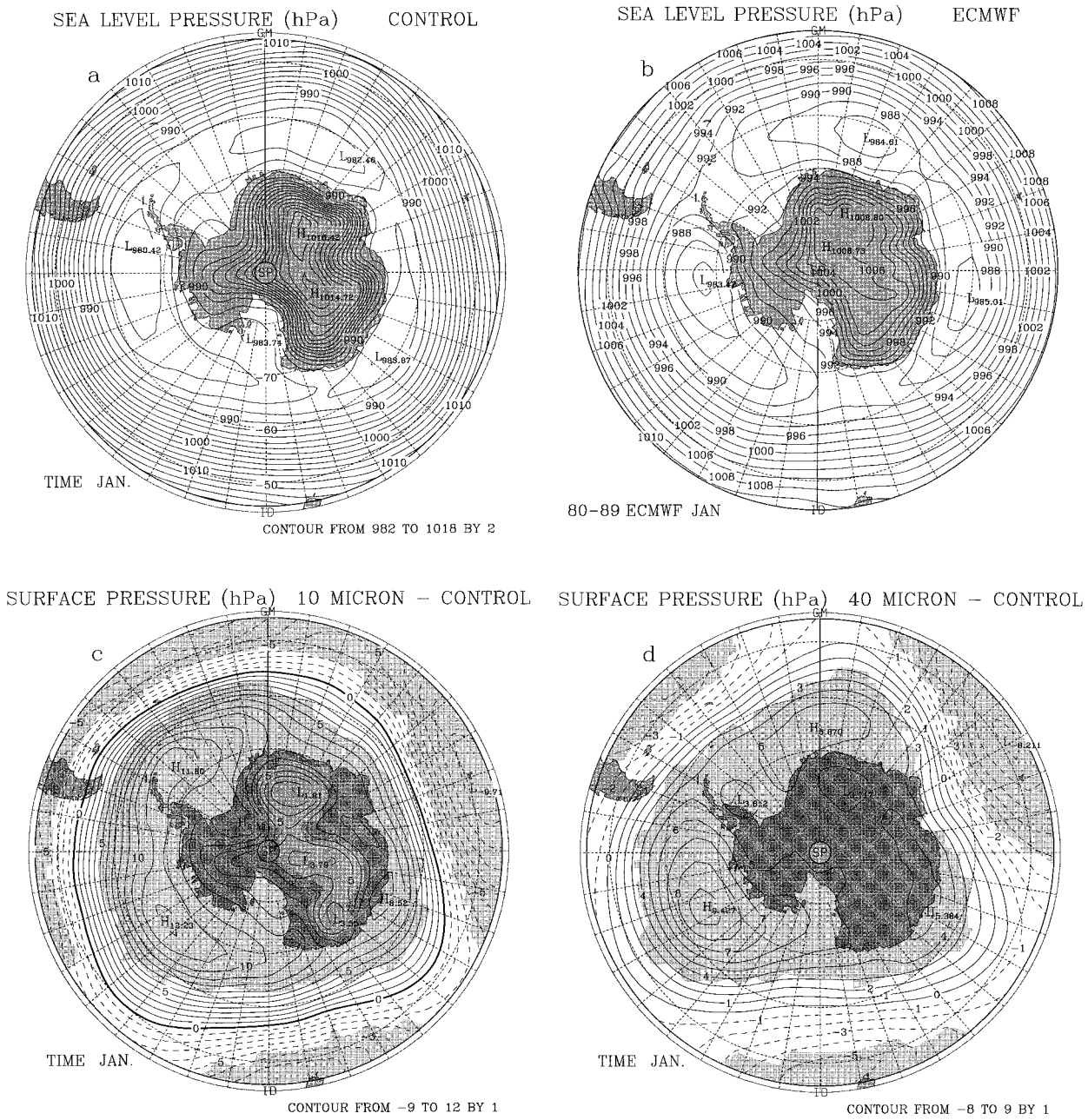

FIG. 8. Same as in Fig. 5 except for sea level pressures (hPa) for (a) control run and (b) observed from 1980–89 ECMWF analyses, and differences in surface pressure (hPa) between (c) 10-μm ice cloud run and control run and (d) between 40-μm ice cloud run and control run. Statistically significant differences in (c) and (d) are stippled at the 95% confidence level.

played in Fig. 13. Unlike the eddy heat fluxes, which are relatively important at both the upper and lower levels of the atmosphere in the middle latitudes but much smaller than the zonal mean components, eddy momentum fluxes are more important in the upper levels of the middle latitudes than the zonal mean momentum fluxes. It is apparent that the centers of poleward eddy momentum transport are reduced in both hemispheres (Figs. 13a and 13b). There are two poleward anomalies of eddy momentum flux centered at about 72°S and 25°S, but equatorward anomalies of the eddy momentum flux between 65°–35°S. In the Northern Hemisphere, the poleward transport anomalies of the eddy momentum fluxes are found to the north of 40°N, and the equatorward transport anomalies are located to the south of 40°N. The distribution of the anomalies of eddy momentum flux in terms of the divergence is well associated with the changes in zonal wind (Fig. 11c). Sim-

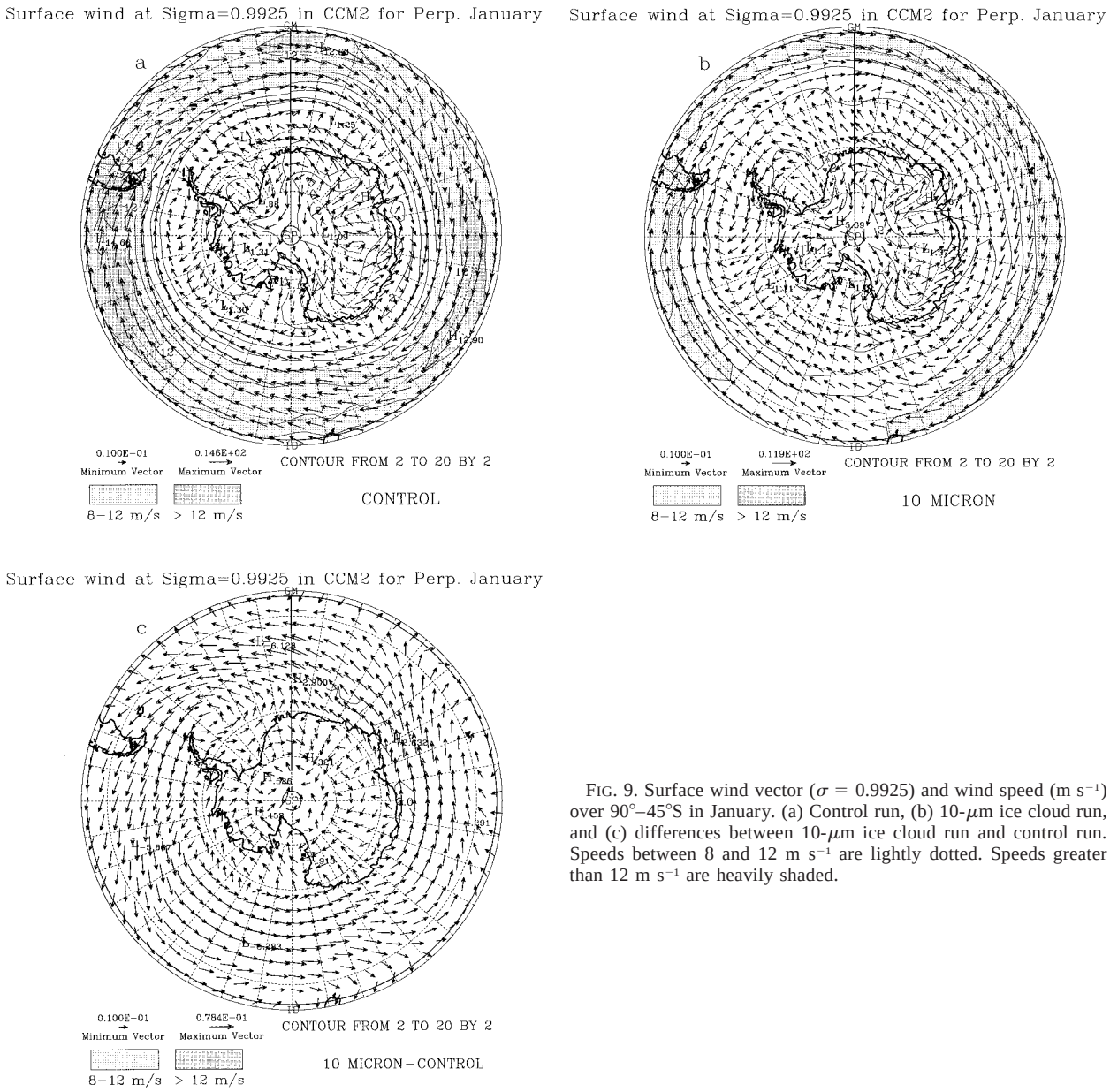

FIG. 9. Surface wind vector ($\sigma = 0.9925$) and wind speed (m s^{-1}) over 90°–45°S in January. (a) Control run, (b) 10-μm ice cloud run, and (c) differences between 10-μm ice cloud run and control run. Speeds between 8 and 12 m s^{-1} are lightly dotted. Speeds greater than 12 m s^{-1} are heavily shaded.

ilar to anomalies of the mean meridional heat flux, the anomalies of the mean meridional momentum flux (figure omitted) are in the same sense as the anomalies in meridional circulation.

5. Impacts on the Tropics

In an evaluation of the greatest impact that sea-ice anomalies around Antarctica could have on the regional and global atmospheric circulation, an extended seasonal cycle integration of CCM2 was conducted in which all Antarctic sea ice was replaced by open water (Bromwich and Chen 1996). They found that there are not only substantial anomalies in various variables in the Southern Hemisphere but also significant changes in the Tropics and the Northern Hemisphere.

In this perpetual January simulation of Antarctic cloud phase and size sensitivity, global anomaly patterns similar to those obtained in the sea-ice removal experiments have been observed (e.g., Fig. 11). Changes in the Tropics would be one of the key issues for exploring global influences from high southern latitudes. Consequently, we examined the mean meridional circulation which is well defined in the Tropics. Wu and Brankovic (1985) calculated the zonally averaged $[\cdot]$ meridional mass flux, χ, in pressure coordinates

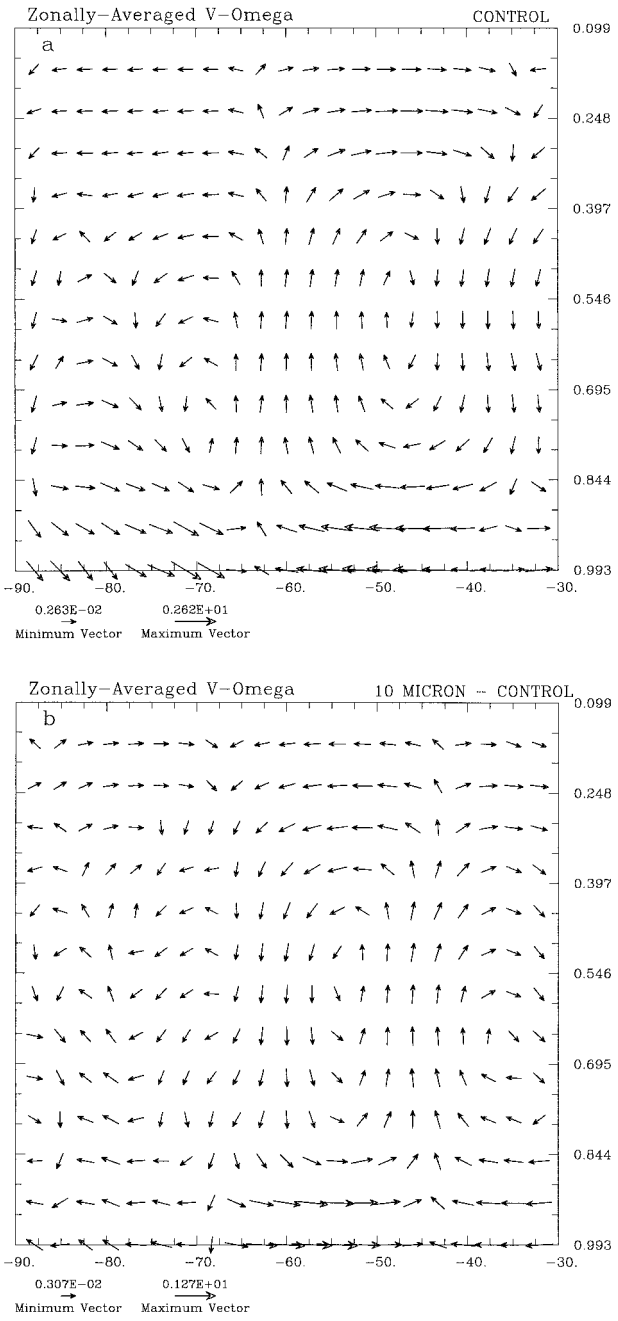

FIG. 10. Zonally averaged cross section of meridional circulation (v–ω) plotted as vectors from 90°–30°S in January for (a) control run and (b) differences between 10-μm ice cloud run and control run. The value of v is in m s^{-1}, and ω is in Pa s^{-1} multiplied by 20.

$$\frac{\partial[\chi]}{\partial\varphi} = \frac{-2\pi a^2}{g}[\omega]\cos\varphi$$
$$\frac{\partial[\chi]}{\partial p} = \frac{2\pi a}{g}[v]\cos\varphi, \qquad (3)$$

where φ is latitude, a is the earth's radius, ω is vertical

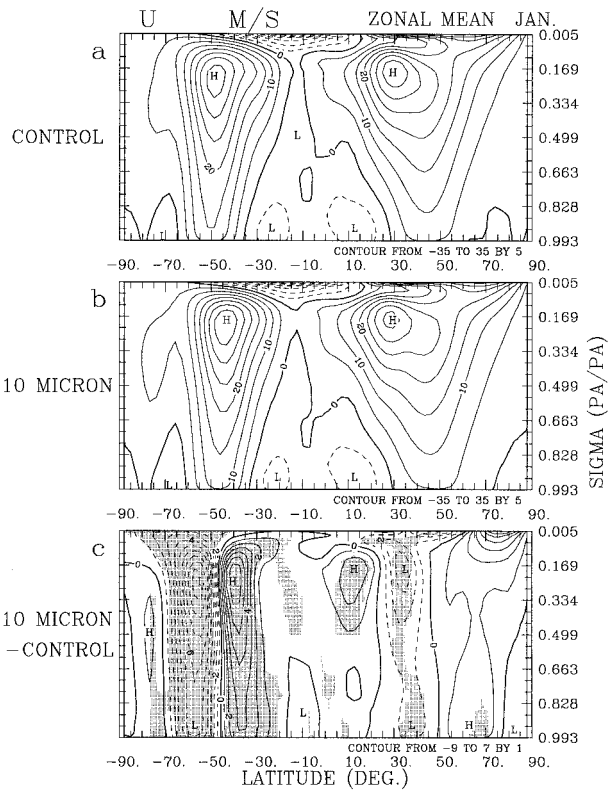

FIG. 11. Zonally averaged cross section of zonal wind component (m s^{-1}) over 90°S–90°N in January for (a) control run, (b) 10-μm ice cloud run, and (c) difference between 10-μm ice cloud run and control run. Statistically significant differences in (c) are stippled at the 95% confidence level.

velocity, v is meridional velocity, and g is gravity. Together with the continuity equation, the χ can be expressed as an analytic function of φ and p:

$$d[\chi] = \frac{\partial[\chi]}{\partial\varphi}d\varphi + \frac{\partial[\chi]}{\partial p}dp. \qquad (4)$$

The value of χ can be found by integrating (4) with appropriate boundary conditions (details given by Wu and Brankovic 1985).

Figure 14 shows the zonal mean meridional mass fluxes for the control and the 10-μm ice cloud runs. There are three meridional circulations in each hemisphere with the tropical Hadley and midlatitude Ferrel circulations being stronger in the Northern Hemisphere winter than in the Southern Hemisphere summer. However, due to the presence of Antarctica and less annual variability in the Southern Hemisphere than in the Northern Hemisphere, the polar circulation in the southern summer is even stronger than the northern winter polar circulation. In comparison with the control run, the circulations in the 10-μm ice cloud run are about 15%–20% weaker and move northward by about 2°–3° latitude. There are statistically significant (>95%) anomalies in the troposphere globally except for the

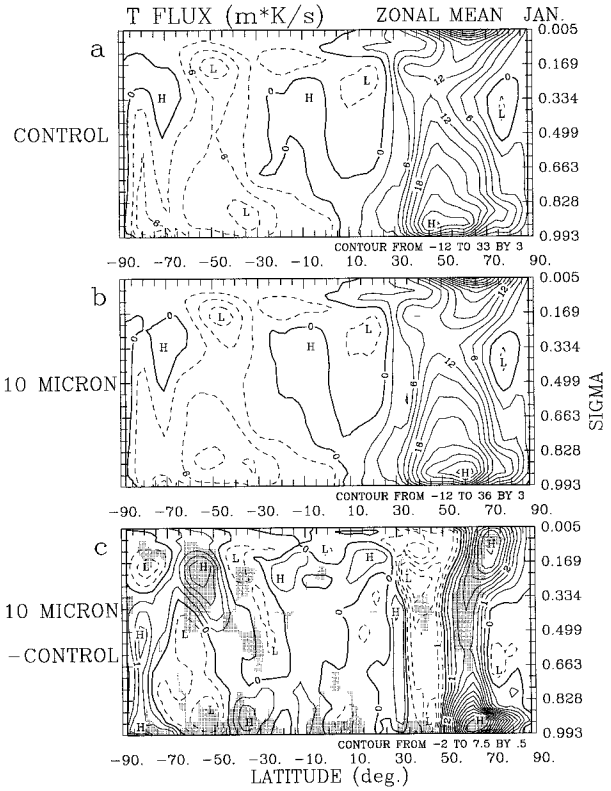

FIG. 12. Same as in Fig. 11 except for meridional eddy temperature flux (K m s^{-1}).

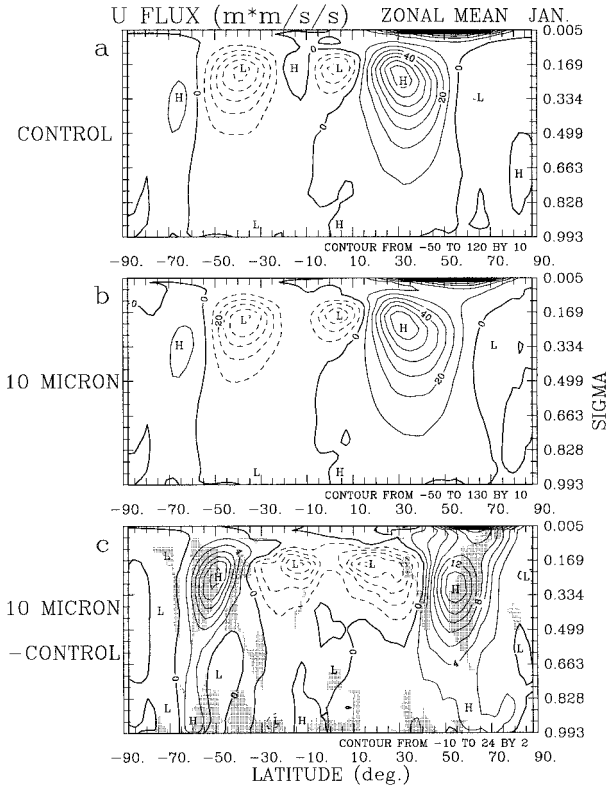

FIG. 13. Same as in Fig. 11 except for meridional eddy momentum flux (m^2s^{-2}).

north polar region. The meridional mean mass flux changes by up to 20% in the Tropics. It is clear that the tropical mean flow is altered substantially when ice clouds are implemented in Antarctica.

The zonally averaged latent heat release is shown in Fig. 15 for the control and 10-μm ice cloud runs. The deepest convection is located in the southern Tropics, while the largest latent heat release from shallow convection and large-scale condensation is in the northern Tropics. Secondary maxima appear in the middle latitudes in both hemispheres. Again, similar to Fig. 11b, the patterns of latent heat release in 10-μm ice cloud run are also shifted equatorward in both hemispheres. It is interesting to note that radiation budget changes in Antarctica (warming in the southern atmospheric heat sink) not only cause circulation adjustments in the Southern Hemisphere but also increase the latent heat release in the upper troposphere between 10° and 30°N. Large and significant responses occur in 70°–30°S, which are associated with anomalies in mean circulation (Fig. 14) and eddies (Figs. 12 and 13) and are consistent with cloud fraction changes (Fig. 4). However, the zonally averaged anomalies in the southern Tropics are not significant in contrast to the southern middle and high latitudes. The characteristics of zonal asymmetry in the Tropics are examined here to further explore the tropical responses to high latitude forcing. Figure 16 shows the 30°S–0° meridionally averaged cross section (longitude versus σ) for latent heat release. There are three major convective latent heat release zones: Africa and Indian Ocean, western Pacific, and South America (Figs. 16a and 16b). The most significant anomalies are negative and occur in the western Indian Ocean, eastern Pacific Ocean, and Atlantic Ocean. This suggests that latent heat anomalies are significant in the Tropics but have high zonal asymmetry. Both observations and theoretical studies (Tomas and Webster 1994; Webster and Holton 1982) indicate that middle latitude disturbances can penetrate into the Tropics and sometimes even propagate into the extratropics of the other hemisphere. These require the existence of tropical westerlies as a ''wave guide'' that are the strongest during winter (January). It is also in the winter hemisphere that circulation anomalies are most prominent (Webster 1983). In these experiments, the most persistent and strongest westerlies in the Tropics are located in the Pacific Ocean and secondarily over South America and the Atlantic Ocean (figure omitted). Coincidentally, the largest anomalies of sea level pressure ($\pm$10 hPa, not shown) in the extratropics of the Northern Hemisphere are found in the Aleutian and Icelandic lows, respectively.

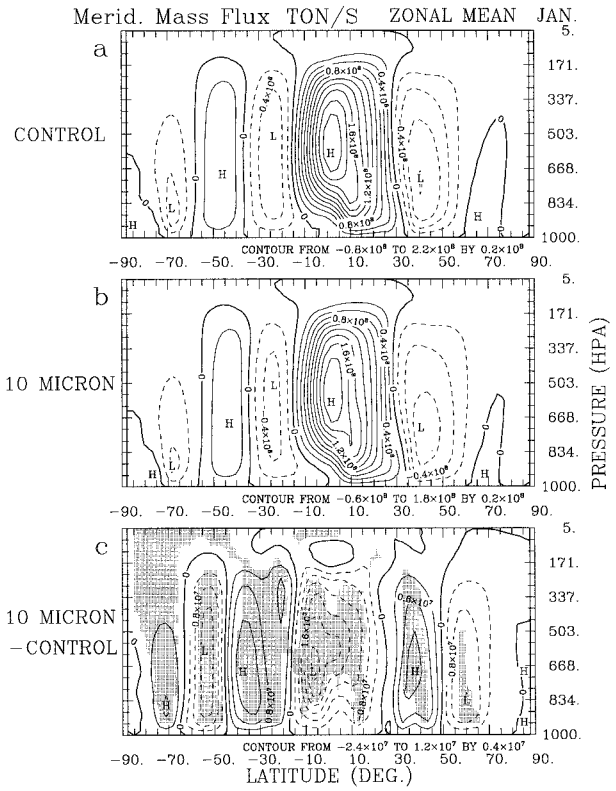

FIG. 14. Same as in Fig. 11 except for meridional mass flux (Ton s^{-1}).

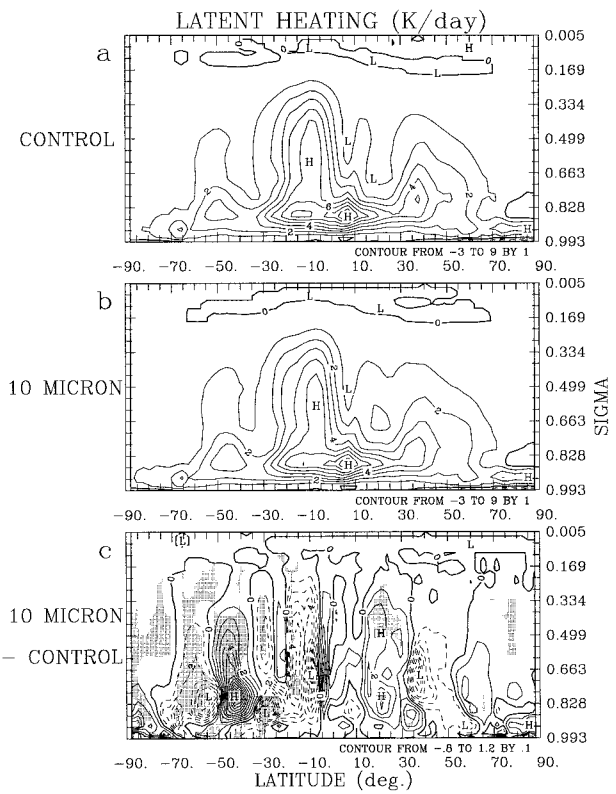

FIG. 15. Same as in Fig. 11 except for latent heat release (K day^{-1}).

The evidence presented here implies that the northern (winter) hemispheric responses to Antarctic radiation forcing presented here are physically consistent. To identify the mechanisms for signal propagation from the Southern Hemisphere into the Tropics and extratropics of the Northern Hemisphere requires detailed analysis that is beyond the scope of this paper.

6. Discussion

In this paper, it has been demonstrated that Antarctic cloud radiative properties in terms of phase and particle size are critical for simulation of the regional climate as well as for far-field impacts. Notice that the two ice cloud experiments conducted in this study are very plausible for the Antarctic summer. It is believed that clouds of supercooled liquid water droplets are present in addition to ice clouds (S. Warren 1996, personal communication). In this regard, CCM3, with the option of allowing mixed-phase cloud particles, will be a better test bed for understanding the impacts of Antarctic cloud properties on climate and for improving the accuracy of simulations. In addition, observations over the Antarctic plateau suggest that our use of up to 40 μm for an equivalent-spherical radius for ice crystals in summer is reasonable (S. Warren 1996, personal communication).

Several different GCM experiments suggest Antarctic forcing affects regional and global climate. In the late 1980s, Rind (1987) found that significant changes in the atmospheric circulation of both hemispheres occurred as ice age boundary conditions were primarily implemented in the Northern Hemisphere of a GCM. In a set of perpetual July simulations evaluating the atmospheric sensitivity to Antarctic sea ice concentration, Simmonds and Budd (1991) displayed statistically significant anomalies of zonal wind and temperature in the Northern Hemisphere summer in addition to large anomalies in the Southern Hemisphere. Recently, Bromwich and Chen (1996) re-evaluated the maximum impacts that Antarctic sea-ice anomalies could have on regional and global climate using the NCAR CCM2 in a seasonal cycle mode. Their simulations revealed substantial changes in various variables in both hemispheres as well as in the Tropics. In the present experiments, equally or even more significant anomalies are observed globally as a result of changes made to the radiative properties of Antarctic clouds. The response is amplified in relation to the real world, because Antarctic cloud amounts are overpredicted by the model (Tzeng et al. 1994).

Based on the results, we hypothesize the cause and effect mechanisms shown in the schematic diagram in Fig. 17. The change in cloud optical properties from those of liquid water to those of ice over the Antarctic

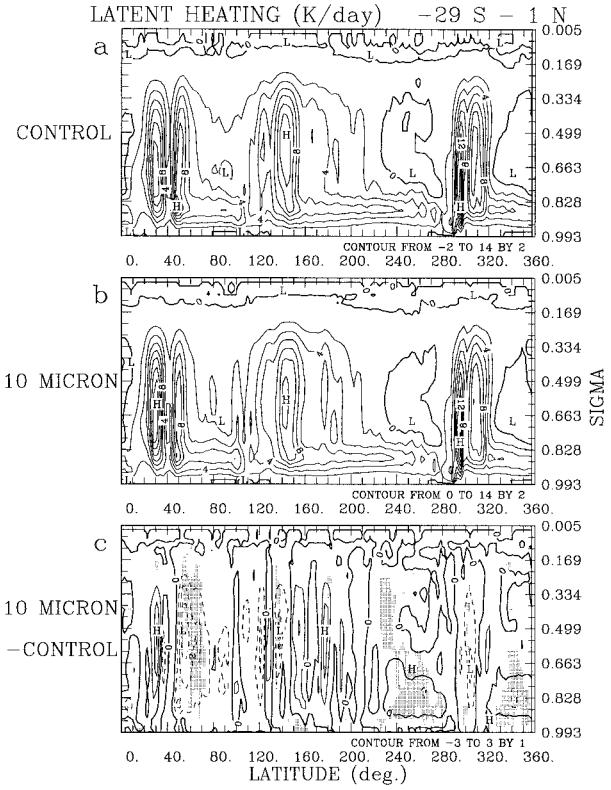

FIG. 16. Cross section averaged over 30°S–0° of latent heat release (K day^{-1}) for (a) control run, (b) 10-μm ice cloud run, and (c) difference between 10-μm ice cloud run and control run. Statistically significant differences in (c) are stippled at the 95% confidence level.

plateau warms the free atmosphere over Antarctica and its vicinity primarily due to the radiative balance. Therefore, the anomalies of north–south temperature gradient are superimposed on the thermal forcing. The equator-to-pole temperature contrast is an essential driving force for the atmospheric circulation. As a result, the intensities and locations of the Antarctic drainage flow, polar meridional circulation, cloud coverage, and circumpolar trough are significantly altered. By indirect thermodynamic and dynamic effects, the Ferrel circulation, storm track, and thermal structure in the middle latitudes also change. The significant changes in the mean flow are accompanied by eddy anomalies (transient and stationary waves). Through wave and mean flow interaction, tropical perturbations in latent heat release and precipitation occur as well. Numerous observational and theoretical studies suggest that tropical anomalies have substantial influences on middle and high latitude climate, especially in the winter hemisphere (Webster 1983); this could explain the anomalies observed in these experiments over the Northern Hemisphere. Together with the other sensitivity simulations to Antarctic forcing, the present experiments suggest that high latitude processes play a more important role in global climate than previously thought.

Acknowledgments. We appreciate extensive discussions with David Rind and Minghua Zhang. Special thanks go to Linjuan Gong for her persistent efforts in processing the simulation data. This research was supported by Grants NASA NAGW-2718 (DHB) and NSF OPP-9414276 (DL). The research of Wan-Ho Lee and

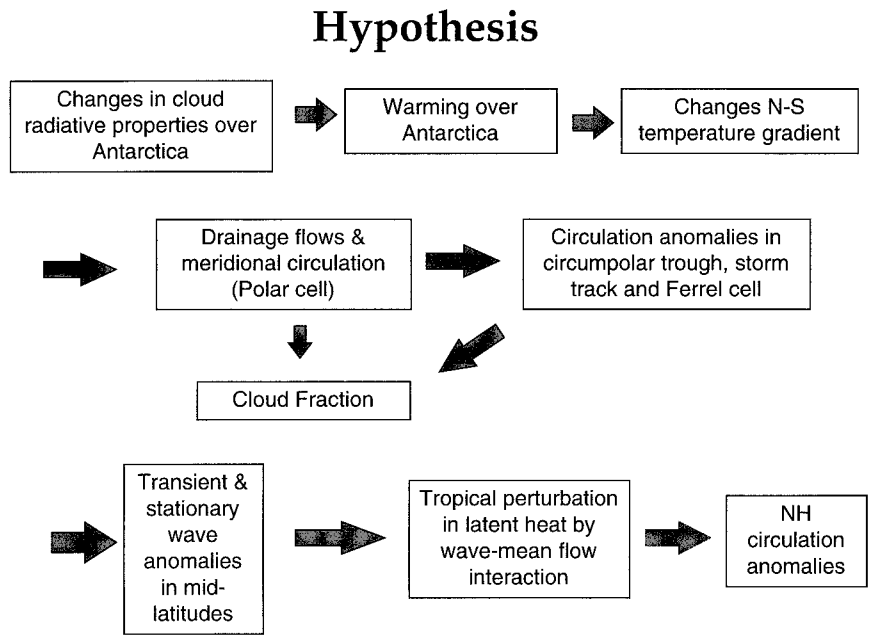

FIG. 17. Schematic hypothesis for mechanisms relating Antarctic clouds to tropical and Northern Hemisphere climate.

Richard C. J. Somerville has been supported in part by Grants NSF ATM-9114109, NASA NAG5-236, and NAG5-2238, NOAA NA90AA-D-CP526, DOE-ARM DE-FG03-90ER61061, and Digital Equipment Corporation 1243, as well as the University of California Institutional Collaborative Research Program. The computations were mostly performed on the CRAY Y-MP of NCAR and in part on the CRAY Y-MP of the Ohio Supercomputer Center.

REFERENCES

Bromwich, D. H., and B. Chen, 1996: Global atmospheric impacts induced by sea ice anomalies around Antarctica. Preprints, *Conf. on the Global Ocean–Atmosphere–Land System (GOALS)*, Atlanta, GA, Amer. Meteor. Soc., 218–222.

——, R.-Y. Tzeng, and T. R. Parish, 1994: Simulation of the modern Arctic climate by the NCAR CCM1. *J. Climate,* **7,** 1050–1069.

Cess, R. D., and Coauthors, 1995: Absorption of solar radiation by clouds: Observations versus models. *Science,* **267,** 496–499.

Chen, B., D. H. Bromwich, K. M. Hines, and X. Pan, 1995: Simulations of the 1979–88 polar climates by global climate models. *Ann. Glaciol.,* **21,** 83–90.

Ebert, E. E., and J. A. Curry, 1992: A parameterization of ice cloud optical properties for climate models. *J. Geophys. Res.,* **97,** 3831–3836.

Hack, J. J., B. A. Boville, B. P. Briegleb, J. T. Kiehl, P. J. Rasch, and D. L. Williamson, 1993: Description of the NCAR Community Climate Model (CCM2). NCAR Tech. Note NCAR/TN-382+STR, Boulder, CO, 108 pp.

Han, Q., W. B. Rossow, and A. A. Lacis, 1994: Near-global survey of effective droplet radius in water clouds using ISCCP data. *J. Climate,* **7,** 465–497.

Hanel, R. A., B. J. Conrath, V. G. Kunde, C. Prabhakara, I. Revah, V. V. Salomonson, and G. Wolford, 1972: The Nimbus 4 infrared spectroscopy experiment, I: Calibrated thermal emission spectra. *J. Geophys. Res.,* **77,** 2629–2641.

Keller, L. M., G. A. Weidner, C. R. Stearns, and M. F. Sievers, 1989: Antarctic automatic weather station data for the calendar year 1988. Department of Meteorology, University of Wisconsin—Madison, Madison, WI, 329 pp. [Available from Dept. of Atmospheric and Oceanic Sciences, University of Wisconsin—Madison, 1225 W. Dayton St., Madison, WI 53706.]

Kiehl, J. T., 1994: Sensitivity of a GCM climate simulation to differences in continental versus maritime cloud drop size. *J. Geophys. Res.,* **99,** 23 107–23 115.

——, J. J. Hack, M. H. Zhang, and R. D. Cess, 1995: Sensitivity of a GCM climate to enhanced shortwave cloud absorption. *J. Climate,* **8,** 2200–2212.

——, B. A. Boville, B. P. Briegleb, J. J. Hack, P. J. Rasch, and D. L. Williamson, 1996: Description of the NCAR Community Climate Model (CCM3). NCAR Tech. Note NCAR/TN-420+STR, Boulder, CO, 152 pp.

Knollenberg, R. G., K. Kelly, and J. C. Wilson, 1993: Measurements of high number densities of ice crystals in the tops of tropical cumulonimbus. *J. Geophys. Res.,* **98,** 8639–8664.

Lee, W.-H., and R. C. J. Somerville, 1996: Effects of alternative cloud radiation parameterizations in a general circulation model. *Ann. Geophys.,* **14,** 107–114.

Lubin, D., 1994: Infrared radiative properties of the maritime Antarctic atmosphere. *J. Climate,* **7,** 121–140.

——, and D. A. Harper, 1996: Cloud radiative properties over the South Pole from AVHRR infrared data. *J. Climate,* **9,** 3405–3418.

——, J.-P. Chen, P. Pilewskie, V. Ramanathan, and F. P. J. Valero, 1996: Microphysical examination of excess cloud absorption in the tropical atmosphere. *J. Geophys. Res.,* **101,** 16 961–16 972.

Morely, B. M., E. E. Uthe, and W. Viezee, 1989: Airborne lidar observations of clouds in the Antarctic troposphere. *Geophys. Res. Lett.,* **16,** 491–494.

Nemesure, S., R. D. Cess, E. G. Dutton, J. J. DeLuisi, Z. Li, and H. G. Leighton, 1994: Impact of clouds on the shortwave radiation budget of the surface–atmosphere system for snow-covered surfaces. *J. Climate,* **7,** 579–585.

Ramanathan, V., E. J. Pitcher, R. C. Malone, and M. L. Blackmon, 1983: The response of a general circulation model to refinements in radiative processes. *J. Atmos. Sci.,* **40,** 605–630.

——, B. Subasilar, G. Zhang, W. Conant, R. D. Cess, J. Kiehl, H. Grassl, and L. Shi, 1995: Warm pool heat budget and shortwave cloud forcing: A missing physics? *Science,* **267,** 499–503.

Rind, D., 1987: Components of the ice age circulation. *J. Geophys. Res.,* **92,** 4241–4281.

Saxena, V. K., and F. H. Ruggiero, 1990: Antarctic coastal stratus clouds: Microstructure and acidity. *Contributions to Antarctic Research I,* Antarct. Res. Series, Vol. 50, Amer. Geophys. Union, 7–18.

Shibata, K., and M. Chiba, 1990: Effects of radiation scheme on the surface and wind regime over the Antarctic and on circumpolar lows. *NIPR Symp. Polar Meteor. Glaciol.,* **3,** 58–78.

Simmonds, I., and W. F. Budd, 1991: Sensitivity of the southern hemisphere circulation to leads in the Antarctic pack ice. *Quart. J. Roy. Meteor. Soc.,* **117,** 1003–1024.

Slingo, A., 1989: GCM parameterization for the shortwave radiative properties of water clouds. *J. Atmos. Sci.,* **46,** 1419–1427.

——, and J. M. Slingo, 1991: Response of the National Center for Atmospheric Research Community Climate Model to improvements in the representation of clouds. *J. Geophys. Res.,* **96,** 15 341–15 357.

Stone, R. S., 1993: Properties of austral winter clouds derived from radiometric profiles at the South Pole. *J. Geophys. Res.,* **98,** 12 961–12 971.

Tomas, R. A., and P. J. Webster, 1994: Horizontal and vertical structure of cross-equatorial wave propagation. *J. Atmos. Sci.,* **51,** 1417–1430.

Tzeng, R.-Y., D. H. Bromwich, T. R. Parish, and B. Chen, 1994: NCAR CCM2 simulation of the modern Antarctic climate. *J. Geophys. Res.,* **99,** 23 131–23 148.

Walden, V. P., 1995: The downward longwave radiation spectrum over the Antarctic Plateau. Ph.D. thesis, University of Washington, 267 pp. [Available from UMI Dissertation Abstracts International, 300 N. Zeeb Road, Ann Arbor, Michigan 48106; UMI AA19616686.]

Webster, P. J., 1983: Large scale structures of the tropical atmosphere. *Large-Scale Dynamical Processes in the Atmosphere,* B. J. Hoskins and R. P. Pearce, Eds., Academic Press, 127–168.

——, and J. R. Holton, 1982: Cross equatorial response to middle-latitude forcing in a zonally varying basic state. *J. Atmos. Sci.,* **39,** 722–733.

Wu, G., and C. Brankovic, 1985: General circulation diagnostics package. ECMWF Res. Dept. Tech. Memo. 96, ECMWF, Reading, United Kingdom, 35 pp.

Yamanouchi, T., and T. P. Charlock, 1995: Comparison of radiation budget at the TOA and surface in the Antarctic from ERBE and ground surface measurements. *J. Climate,* **8,** 3109–3120.

Zav'yalova, I. N., 1986: Humidity of air in Antarctica. *Climate of Antarctica,* I. M. Dolgin, Ed., Oxonian Press, 92–101.